

Aeolian erosion thresholds for cohesive sand

J-B. Besnard^{1,2}, P. Dupont², A. Ould El Moctar³, A. Valance¹

¹Univ Rennes, CNRS, Institut de Physique de Rennes, UMR 6251, 35 042 Rennes, France

²Univ Rennes, INSA Rennes, LGCGM, 35 043 Rennes, France

³Univ Nantes, CNRS, Laboratoire Thermique et Energie, UMR 6607, 44306 Nantes Cedex, France

Key Points:

- We devised a new approach to assess the aerodynamic and dynamic transport thresholds for cohesive sand beds in wind-tunnel experiments.
- The aerodynamic threshold is found to increase linearly with the amount of liquid content within the sand bed.
- Unlike the aerodynamic threshold, the dynamic threshold remains unchanged in the range of cohesive strength investigated so far.

Abstract

Moisture is known to affect sand cohesion and therefore transport threshold and rate of aeolian sand transport. Aeolian sand transport has been widely documented for dry sand beds, but much more sparsely in the context of moist sand beds. One major challenge in the collection of reliable field or laboratory data for moist sand is to have an accurate control of the moisture level within the sand bed, which is prone to strongly vary over time and space due to evaporation. To suppress the variability of moisture content due to evaporation, we devised a new approach based on the use of a non-volatile liquid (namely silicon oil instead of water) which ensures a proper control of the liquid content. We thus conducted wind-tunnel experiments employing this approach and observed that the aerodynamic threshold friction velocity increases linearly with liquid content, while the dynamic threshold is found to be unchanged in the range of cohesion strength investigated in this study. These outcomes indicate that the difference between the static and dynamic threshold increases with increasing cohesion. This may have strong implications on aeolian transport of moist sand, and in particular on hysteretic behaviors.

Plain Language Summary

Moisture has a significant influence on the initiation of motion of sand by wind and also on the resulting sand transport rate. While the moisture level is usually very low in sandy desert areas and thus irrelevant there, the aeolian sand transport on sandy beaches or in the context of coastal dune morphodynamics is expected to be crucially dependent on the moisture content within the sand. The literature regarding the impact of the moisture on wind blown sand is sparse, and available data exhibit considerable discrepancies regarding the magnitude of the moisture effects. These discrepancies highlight that it is experimentally difficult to control the moisture levels within the sand because of evaporation. To circumvent this difficulty, we carried wind-tunnel experiments with sand-oil mixtures instead of sand-water mixtures. Oil plays the same role as water in generating cohesion but has the significant advantage to have a very low evaporation rate in the standard conditions of temperature and pressure. With these sand-oil mixtures, we were able to assess with an unprecedented accuracy the magnitude of the cohesion effects on the aerodynamic erosion threshold and also on the threshold characterizing the cessation of transport, known as the dynamic threshold.

1 Introduction

Aeolian processes that involve the entrainment, transport, and deposition of sediment by the wind are important geomorphic processes operating in arid regions but also along sandy shores. They are responsible in particular for the formation and migration of sand dunes. Understanding these processes in complex environments (e.g., in the presence of vegetation or in the context of cohesive soils) demands further investigations.

Wind blown sand involves a myriad of physical mechanisms, including particle-particle, bed-particle and fluid-particle interactions. A comprehensive quantification of these interactions in the context of cohesive particulate beds remains a scientific challenge. Aeolian sand transport with non-cohesive particles can be regarded as one of the simplest air-particulate flows, while the transport of moist sand or snow exhibits a much greater complexity.

The complexity of the aforementioned real cohesive systems arises from the fact that the strength of the cohesion may strongly evolve in time and space. Monitoring these variations in situ at the relevant temporal and spatial scales is beyond of the classical instrumental capabilities. Promising instruments based on capacitance measurements (Louge et al., 2010, 2013, 2022) are however, capable of monitoring tiny variations of moisture content at the surface of a sand bed and within the bed with a centimetric spatial resolution and should be further deployed on the field or in wind tunnel experiments to better document the coupling between sand transport and cohesion. This capacitance technique has already proven to be effective to probe the temporal evolution of the water content within a barchan dune (Louge et al., 2013,

2022). Also, the potential effects of inter-particle cohesion on the transfer of mass, momentum and energy between the moving particles and the static bed remain poorly documented (Namikas & Sherman, 1995). Thus, predicting mass transport rates for these complex systems is very uncertain.

An important issue in wind-blown sand concerns the critical air flow velocity at which transport starts and ceases. These thresholds are referred to as the aerodynamic and dynamic thresholds, respectively (Bagnold, 1941; Kok & Rennó, 2009; Duran et al., 2011; Valance et al., 2015; Pähtz et al., 2020). Different physical interpretations of the dynamic threshold can be found in the literature. Some authors (Pähtz et al., 2020, 2021) interpret the latter as the rebound threshold, describing the smallest wind friction velocity to sustain a continuous saltation motion of a single grain along the bed. This hypothesis is independent of the ejection process, but related to the properties of the rebound. Other ones (Duran et al., 2011; Jenkins & Valance, 2014; Valance et al., 2015) define the dynamic threshold to be the minimum wind speed to sustain a non-zero saturated flux. In the latter perspective (as detailed further below), the dynamic threshold is related to the splash process and the replacement capacity.

For dry aeolian sand of $200\ \mu\text{m}$ size, the dynamic threshold is significantly smaller (20% less (Bagnold, 1941; Ho, 2012)) than the aerodynamic one and this is due to the fact that once transport has been initiated, erosion induced by the impact of grains onto the bed is a very efficient mechanism to sustain the saltation transport (Beladjine et al., 2007; Creyssels et al., 2009). This hysteretic effect between initiation and cessation is expected to be drastically modified for cohesive beds as suggested by the recent numerical work from Comola, Gaume, et al. (2019) which showed in the context of snow transport that saltation over cohesive beds sustains itself at wind speeds 1 order of magnitude smaller than those necessary to initiate it. We shall also mention a recent experimental work in a closed-loop wind-tunnel by Andreotti et al. (2021) which questions the existence of two distinct thresholds. They did not observe any difference between the aerodynamic and dynamic thresholds when increasing or decreasing the wind strength and ascribe this outcome to the essential role of the turbulent flow velocity fluctuations, which are probably strongly enhanced by the closed-loop wind-tunnel.

Most of the studies dedicated to transport of moist sand focused on the modification of the aerodynamic threshold with the moisture level (Chepil, 1956; Belly, 1962; Bisal & Hsieh, 1966; Hotta et al., 1984; McKenna-Neuman & Nickling, 1989; Cornelis et al., 2004a; Han et al., 2009). The presence of moisture in sand is known to create cohesive forces between grains and has thus a strong influence on the initiation of sand transport which requires higher wind strengths. The aerodynamic threshold, also referred to as the static threshold, is defined as the minimum wind friction velocity to set grains into motion from a resting situation (Bagnold, 1941). For a cohesionless sand bed, the transport is initiated when the friction velocity overpasses a critical value u_s^* given by

$$u_s^* = A \sqrt{\frac{(\rho_p - \rho_f)}{\rho_f} gD}, \quad (1)$$

where D is the mean grain diameter, ρ_p and ρ_f are the particle and fluid density, respectively, and A is an empirical coefficient of order of 0.1 (Bagnold, 1941). This relationship can be inferred from a simple force balance between the aerodynamic force and the weight exerted on a grain at the sand bed surface. A typical value of the aerodynamic threshold for dry sand obtained in wind-tunnel is $u_s^* = 0.21\ \text{m/s}$ for sand grains with a mean diameter $D = 0.2\ \text{mm}$ (Ho et al., 2011). It is worth mentioning that the aerodynamic threshold is experimentally difficult to assess because the latter is sensitive to additional parameters that are not easy to properly control or characterize, like the level of the turbulent fluctuations of the air flow or the disorder at the surface of the bed (Duran et al., 2011). As an example, Pähtz et al. (2018) emphasize that the thickness of the turbulent boundary layer plays an important role in the initiation of sand transport and consequently, the aerodynamic threshold measured in natural conditions is often smaller than that measured in wind-tunnel experiments.

111 For moist sand, the aerodynamic threshold is an increasing function of the water con-
 112 tent, but the literature presents a wide spectrum of results regarding the magnitude of mois-
 113 ture effects on the aerodynamic threshold. From wind-tunnel experiments with 0.44 mm sand
 114 grains, Belly (1962) reported a logarithmic evolution of the static threshold friction velocity
 115 with the water content ω (expressed in percent) from $\omega \approx 0.046\%$ to $\omega = 4\%$:

$$u_{sw}^* = u_s^* (1.8 + 0.6 \log \omega) . \quad (2)$$

116 In contrast, Hotta et al. (1984) proposed a linear relationship also on the basis of wind-tunnel
 117 experiments which is verified up to $\omega = 8\%$:

$$u_{sw}^* = u_s^* (1 + a_H \omega) . \quad (3)$$

118 The authors found that the slope a_H decreases with increasing grain diameter D : $a_H \approx 0.94, 0.30$
 119 and 0.22 for $D = 0.2, 0.5$ and 0.8 mm, respectively. As highlighted by Hotta et al. (1984),
 120 the great diversity in the experimental data regarding the effect of the moisture on the aero-
 121 dynamic threshold illustrates the difficulty of controlling the moisture levels within the bed due
 122 to evaporation. To mitigate the evaporation process, some of the wind-tunnel experiments were
 123 conducted with a saturated air flow, as done by Belly (1962), McKenna-Neuman and Nick-
 124 ling (1989) and V. J.-L. Ralaiarisoa (2020). However, it is quite difficult to maintain an air
 125 flow at saturation (i.e., $RH = 100\%$). As a consequence, the water content of the sand bed
 126 and in particular within the first layers of the surface is rapidly varying in space and time ei-
 127 ther through evaporation (under-saturated air) or condensation (over-saturated air), resulting
 128 in an erroneous estimation of the actual water content of the sand surface at the precise in-
 129 stant when sand transport is triggered. Recent experiments (V. J.-L. Ralaiarisoa, 2020) reported
 130 an intermittent transport regime completely controlled by cyclic evaporation of the superficial
 131 layers of the sand bed.

132 Some theoretical models were developed to predict the modification of the static thresh-
 133 old due to cohesion. McKenna-Neuman and Nickling (1989) derived an expression for the crit-
 134 ical shear velocity using a force balance between the grain weight P_g , the cohesive force F_c
 135 and the wind shear stress:

$$u_{sw}^* = u_s^* \sqrt{1 + \alpha Co} , \quad (4)$$

136 where $Co = F_c/P_g$ is the dimensionless cohesion number and α is a constant geometrical
 137 parameter ($\alpha \approx 3$). This relationship is similar to that proposed by Shao and Lu (2000). To
 138 take benefit of the above relationship, the knowledge of the cohesive force F_c at the grain scale
 139 and its dependence on the water content is required, which is an experimental challenge with
 140 grains of submillimeter size. More elaborated expressions can be found in the literature (Cornelis
 141 et al., 2004b; Claudin & Andreotti, 2006). Eq. 4 is however useful to infer the strength of the
 142 cohesion from the assessment of the static threshold friction velocity u_{sw}^* .

143 The other important threshold in wind-blown sand is the dynamic threshold, also referred
 144 to as the impact threshold. According to Duran et al. (2011) and Valance et al. (2015), we de-
 145 fine it as the minimal friction speed u_d^* for which a non-zero saturated flux can be sustained.
 146 A practical method to determine it is to extrapolate to zero the curve relating the sediment flux
 147 to the shear velocity (cf Eq. 5). It is thus defined in a much more accurate manner than the
 148 static threshold, for which a somewhat arbitrary criterion for the onset of particle motion has
 149 to be chosen. The key point explaining this dynamic threshold is the ability of grains in salta-
 150 tion to eject other grains, the so-called splash process (Kok & Rennó, 2009; Duran et al., 2011;
 151 Valance et al., 2015). This process is a statistical process, with a wide distribution of veloc-
 152 ities and angles. In a steady state of transport, the distribution of grain velocities is station-
 153 ary and on average, each saltating grain produces a single saltating grain after a collision with
 154 the bed, either by rebound or by ejection: the capture by the bed of low energy grains that have
 155 a probability to stop is balanced by the ejection of new grains by high energy impacts. One
 156 can formally define the replacement capacity as the average number of saltating grains pro-
 157 duced per collision. At equilibrium, the replacement capacity is exactly 1. In this perspective,
 158 the dynamic threshold is crucially dependent on the splash process. The sand transport model

developed in (Creyssels et al., 2009) that incorporates explicitly the key features of the splash process indicates that the dynamic threshold is intimately linked to the critical impact velocity to trigger the ejection process. As mentioned previously, an alternative interpretation of the dynamic threshold based on the rebound threshold was proposed (Pächtz et al., 2020, 2021) and is still unclear which is the more relevant to describe the saturated transport state at vanishing flux. The dynamic threshold is smaller than the static one and is about 80% of the latter (Bagnold, 1941; Ho, 2012) in the context of aeolian sand transport on earth with 200 μm grain size.

The difference between the static and dynamic threshold is in particular crucially dependent on the grain to fluid density ratio as mentioned by Duran et al. (2011). This difference leads to bi-stability and hysteric behaviors when the wind friction velocity lies between the dynamic and static threshold (Martin & Kok, 2018; Comola, Kok, et al., 2019). Indeed, two stable states can coexist: a state with no transport and another one with a finite mass flux. The latter state can be only obtained with specific boundary or initial conditions (e.g, with a finite upwind mass flux or starting from a transport state with $u^* > u_s^*$ and decreasing the friction speed below u_s^*).

Importantly, the dynamic threshold is a key parameter of the transport law (Duran et al., 2011; Valance et al., 2015). The transport law quantifies the transport capacity of the turbulent air flow as a function of the wind shear stress in the equilibrium state, i.e., when erosion is exactly balanced by deposition. The mass flow rate at equilibrium is usually referred to as the equilibrium or saturated flux (Duran et al., 2011; Valance et al., 2015). For cohesionless sand beds, it scales linearly with the Shields number $S^* = \rho_f u^{*2} / (\rho_p - \rho_f) g D$ (Duran et al., 2011; Valance et al., 2015)

$$Q_{sat} = A_Q \rho_p D u_d^* (S^* - S_d^*), \quad (5)$$

where S_d^* is the critical Shields numbers corresponding to the dynamic friction threshold u_d^* and A_Q is a numerical constant. This linear scaling holds in the saltation regime, but breaks down for very strong winds (i.e., $S^* > 10S_d^*$) (J.-L. Ralaiarisoa et al., 2020).

Two important unresolved issues then arise: how the dynamic threshold is altered in the presence of cohesion and how the transport law is modified? In contrast to the static threshold, the modification of the dynamic threshold in the presence of cohesion has not received a lot of attention. There are very few studies on this issue. We are not aware of experimental studies aiming at determining the dynamic transport threshold as a function of the level of moisture. We can however mention two recent related numerical studies: the work by Comola, Gaume, et al. (2019) which investigates the splash process in the context of snow transport and the one by V. Ralaiarisoa et al. (2022) dedicated to the numerical study of the impact process on cohesive granular packings in the context of aeolian transport for moist sand. The main difference between these two studies is the nature of the cohesion. In the former one, the cohesion is ensured by solid (ice) bonds and the bond breakage is irreversible. In contrast, in the latter study, bonds are water capillary bridges and the breakage is reversible. One of the salient results in (V. Ralaiarisoa et al., 2022) is that the critical impact velocity to trigger the ejection process and its efficiency (i.e., the number of ejected particles per impact) are modified when the cohesion number exceeds a critical value of order 5. Numerical simulations from Comola, Gaume, et al. (2019) confirm that for high cohesion, the efficiency of the ejection process is substantially decreased. These numerical findings thus suggest that for strong cohesion, the dynamic transport threshold should be enhanced. Experimental evidences are however lacking. Concerning the modification of the equilibrium mass flux in the context of cohesive beds, there is no definite answer (McKenna-Neuman & Maljaars, 1998; Davidson-Arnott et al., 2008) due again to the difficulty to conduct experiments with an accurate control of the cohesion within the bed. The limit case corresponding to infinite cohesion (i.e., a rigid bed) is well documented. The experimental study from Ho et al. (2011) reported that the transport capacity over a rigid bed is much greater than over an equivalent erodible bed because the rebound is less dissipative. This was confirmed and explained through a simple two-phase transport model based on periodic trajectories (Jenkins & Valance, 2014). Consequently, as suggested by Davidson-Arnott et al. (2008), we may expect that for large cohesion strength, the saturated flux should

211 overpass the one corresponding to the cohesionless case. The numerical simulations from Comola,
 212 Gaume, et al. (2019) achieved in the context of snow transport provide some indications about
 213 the equilibrium mass flux for cohesive beds. Their results indicate that the equilibrium (i.e.,
 214 saturated) mass flux increases with increasing but rather moderately: for very strong cohesion
 215 (i.e., $Co \approx 10^4$), the flux is found to increase only by a factor 1.25 in comparison with the
 216 cohesionless case.

217 The last important issue concerns the equilibrium length (resp. time) needed to reach
 218 the equilibrium state from a rest state. For the cohesionless case, several studies were devoted
 219 to this complex issue (Andreotti et al., 2010; Selmani et al., 2018). The general belief is that
 220 the equilibrium length increases with increasing the cohesion strength, but there are very few
 221 experimental quantitative studies on this question (Davidson-Arnott et al., 2008; V. J.-L. Rala-
 222 iarisoa, 2020). This belief was however confirmed recently by the numerical simulations from
 223 Comola, Gaume, et al. (2019). The increase of the equilibrium length with increasing cohe-
 224 sion can be explained by the lower efficiency of the splash process (i.e., production of ejected
 225 particles) with cohesive beds as argued by Comola, Gaume, et al. (2019).

226 We propose here an original experimental approach to determine both the static and dy-
 227 namic threshold in the context of cohesive sand beds in an unprecedented controlled manner.
 228 This approach allows getting rid of the evaporation process and to control with accuracy the
 229 cohesion strength of the sand bed. The use of silicon oil instead of water offers the great ad-
 230 vantage of suppressing evaporation. We conducted wind-tunnel experiments based on this ap-
 231 proach and quantified how the aerodynamic and dynamic thresholds vary with the liquid con-
 232 tent.

233 The article is organized as follows. Section 2 describes the experimental facility and the
 234 approach employed to determine both the aerodynamic and impact erosion rates from which
 235 we deduce the aerodynamic and dynamic transport thresholds. In section 3 and 4 we present
 236 the results on aerodynamic and impact erosion rates and discuss the influence of the cohesion
 237 strength of the sand bed on the respective erosion thresholds. Section 5 summarizes the out-
 238 come results and presents outlooks.

239 **2 Experimental setup**

240 **2.1 Wind-tunnel facility**

241 The experiments were carried out in a wind tunnel with a 6.6 *m* length working section
 242 and a 0.245 *m*×0.27 *m* cross-section (see Figure 1). We used as a cohesive sand bed a mix-
 243 ture of 0.2 *mm* sand and silicone oil (*AR* 20) with a surface tension $\Gamma = 20.6 \cdot 10^{-3} \text{ N/m}$. The
 244 sand bed is reduced to a box with a square section of dimensions 0.15 *m*×0.15 *m* and a 0.02 *m*
 245 depth. We chose a small bed sample to get a local evaluation of the erosion rate. The require-
 246 ment is that the length of the sample be much smaller than the saturation length but not too
 247 small for statistical representative measurements. We will come back to the influence of the
 248 bed length on the experimental outcomes in sections 4 and 5.

249 The sand bed sample is placed 5.4 *m* downstream the entrance of the wind tunnel and
 250 its surface is at the same level as the wind-tunnel floor so that there is no discontinuity. The
 251 floor of the wind tunnel (i.e., upstream and downstream of the sand bed) was made rough by
 252 gluing sand particles of the same nature as the sand bed. The sand bed is weighed contin-
 253 uously during the experiment by means of a scale with a milligram accuracy. This allows to
 254 record the erosion rate in the course of time (see further details in section 3).

255 The air flow velocity profile upstream the sand bed was characterized with Pitot tubes
 256 displayed at 10, 15, 20, 25, 30 and 40 mm above the tunnel floor. The profile obeys a clas-
 257 sical logarithmic law

$$U(z) = \frac{u^*}{\kappa} \ln \frac{z}{z_0}, \quad (6)$$

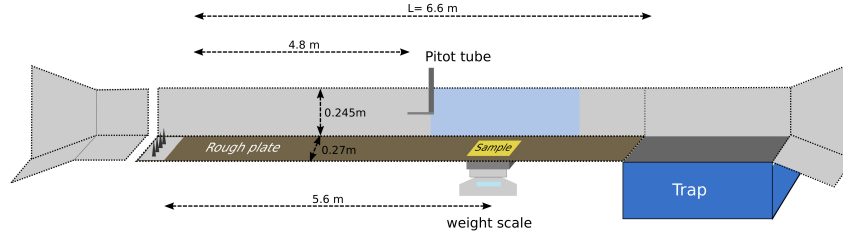


Figure 1. Wind-tunnel facility

258 while the friction velocity u^* follows a linear trend with the free stream velocity U_∞

$$u^* = 0.0388 U_\infty \quad (7)$$

259 and the aerodynamic roughness length z_0 is roughly constant and equal to $z_0 \approx 4.10^{-6} m \approx$
 260 $D/50$.

261 2.2 Sand-oil mixture elaboration

262 Several sand-oil mixtures of about 1 kg were elaborated with various liquid content rang-
 263 ing from $w = 0.025\%$ to $w = 0.4\%$. Each mixture was prepared in a large container and
 264 homogenized manually using a metal rod. The mixture is then poured layer by layer in the
 265 dedicated box. Each layer is about 5 mm height and is smoothed out by a level rake before
 266 pouring the next layer. The particle volume fraction of the obtained packing slightly decreases
 267 with increasing liquid content (see Table 1). However, the decrease is relatively weak except
 268 for the two largest liquid contents ($\omega = 0.3\%$ and 0.4%). For $\omega = 0$, we obtained a vol-
 ume fraction of $\phi = 0.558$ while for $\omega = 0.2\%$, we get $\phi = 0.545$.

$\omega(\%)$	0	0.025	0.05	0.075	0.1	0.2	0.3	0.4
ϕ	0.558	0.559	0.556	0.551	0.551	0.545	0.520	0.500

Table 1. Mixtures used in the experiments and corresponding volume fractions of the sand packings.

269

270 2.3 Upstream conditions

271 We used two different protocols to determine the static and dynamic threshold described
 272 below. For the assessment of the static threshold, the upstream air flow is free of particles and
 273 the air flow velocity is increased by successive incremental steps. A prescribed air flow ve-
 274 locity is set for a duration of 10 minutes and the mass of the packing is recorded in real time
 275 during the run. If the run led to a finite erosion of the sand bed, the packing is rebuilt entirely
 276 for the next run. If not, the air flow velocity is incremented using the same packing. When
 277 a packing is newly built, the first process is to raise the wind speed above the transport thresh-
 278 old for a short time in order to remove the unstable grains lying at the surface of the pack-
 279 ing (McKenna-Neuman & Nickling, 1989).

280 For assessing the dynamic threshold, similar experiments were conducted but a given
 281 incoming particle flux at the entrance of the wind-tunnel. To do this, a hopper filled with dry
 282 sand was placed on the roof of the tunnel at 0.5 m downstream the entrance. The hopper
 283 was designed to feed the air flow with a constant and small incoming sand flux $Q_{in} \approx 48 g/s$. We

284 used a sufficient small incoming flux which can be transported by weak winds, that is with
 285 speeds lower than the dynamic threshold obtained with a cohesionless erodible bed. The sand
 286 bed is then subject to a finite impacting flux Φ that depends both on Q_m and the air flow ve-
 287 locity. This procedure allows assessing the erosion rate by impact and to infer the dynamic
 288 transport threshold as explained in further details in Section 4.

289 3 Aerodynamic erosion

290 3.1 Temporal variation of the erosion rate

291 The continuous recording of the mass M of the sand bed allows determining the tem-
 292 poral evolution of the erosion rate during a given experiment, achieved with a prescribed wind
 293 speed. The erosion rate E is defined as

$$E = -\frac{1}{S} \frac{dM}{dt} \quad (8)$$

294 where S is the surface area of the sand bed. Our measurements reveal that is constant during
 295 the first stage of the erosion process. In a second stage, the erosion rate decreases with time,
 296 corresponding to the moment where the bed surface is no longer flat due to scouring effects
 297 at the downwind of the bed. The second stage occurs when the cumulative mass loss exceeds
 298 approximately $\Delta M \approx 4 \text{ g}$ (Note that a single layer of grains is a bit less than 1 g). In the fol-
 299 lowing, we disregard the second stage of the erosion and infer the erosion rate only from mea-
 300 surements taken in the first stage of the erosion process. The erosion rate is thus calculated
 301 via the slope of the curve $M(t)$ in the linear regime.

302 3.2 Erosion rate versus Wind speed

303 We have measured the erosion rate as a function of the wind strength for sand beds with
 304 various liquid contents, ω ranging from 0.025% to 0.2%. For higher liquid contents (i.e., $\omega =$
 305 0.3 and 0.4) we were not able to reach the transport threshold which was beyond the maxi-
 306 mum wind speed we can reach in our wind-tunnel (i.e., $U_\infty \approx 25 \text{ m/s}$ corresponding to a
 307 friction velocity $u^* \approx 1 \text{ m/s}$). The data presented in Fig. 2.a indicate that for a given liquid
 308 content, the erosion rate follows an exponential growth with the wind friction speed u^* :

$$E = A_e \exp\left(\frac{u^*}{u_e^*}\right), \quad (9)$$

309 where u_e^* is the characteristic friction velocity of the exponential growth (see Fig. 2.b).

310 The exponential behavior suggests that transport could be initiated at a vanishing fric-
 311 tion velocity if one waits for an infinite time. The origin of the exponential trend is not clear
 312 to us, but could be possibly ascribed to the turbulent fluctuations of the air flow. This result
 313 then leaves us with the unresolved issue of how to determine a static threshold with a rele-
 314 vant criterion in the experiments. Stout and Zobeck (1996) indeed, emphasized that the de-
 315 termination of a threshold is dependent on the time of the measure. They also indicate that
 316 although the threshold is sensitive to the time of the measure, it remains finite. These argu-
 317 ments suggest that the experimental assessment of the aerodynamic threshold of transport may
 318 depend on the set-up and experimental procedure.

319 Here, we define the aerodynamic threshold as the erosion rate E overcomes a definite
 320 critical value E_c . We chose a critical value $E_c = 4.10^{-3} \text{ g/m}^2\text{s}$, that corresponds roughly to
 321 a mass loss $\Delta M \approx 5.410^{-2} \text{ g}$ within 10 mn (which is the typical experiment duration). We
 322 selected this value because it is just above the accuracy of the weigh scale. A different choice
 323 for the critical value E_c would of course affect the assessment of the transport threshold but
 324 in the range of less than 10% variation. Using the above criterion, we determine the aerody-
 325 namic threshold for our various cohesive sand beds (see Fig. 3). We find that the static thresh-
 326 old friction velocity increases linearly with the liquid content:

$$u_{sw}^* = u_s^* (1 + a_\omega \omega), \quad (10)$$

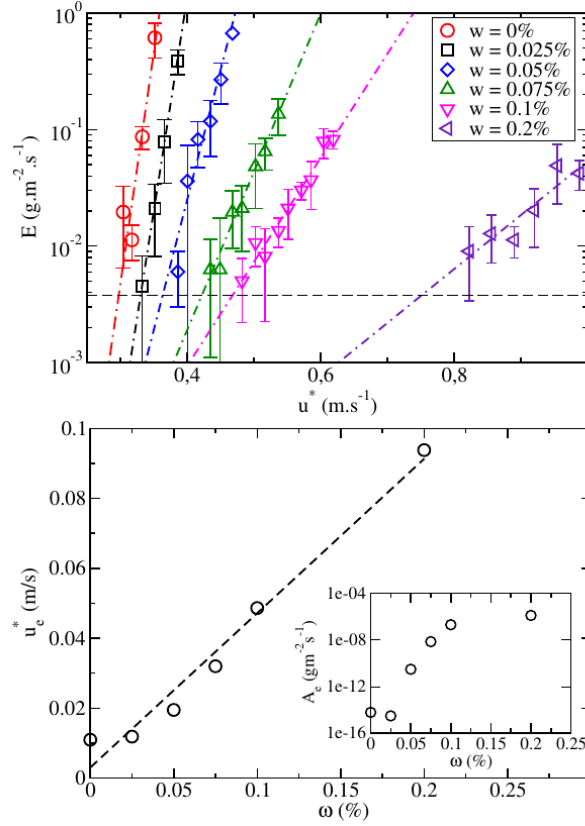


Figure 2. (a) Erosion rate E as a function of the friction speed u^* for different liquid content w . The dash-dotted lines represent exponential fits to the data. The horizontal dash line stands for the critical value of the erosion rate E_c used to define the threshold friction velocity to initiate transport. (b) Characteristic friction velocity u_e^* (see Eq. 9) as a function of ω . Inset: Amplitude A_e of the exponential growth as a function ω .

327 with $a_\omega \approx 7 \pm 0.5$. The static threshold for cohesionless sand (i.e., $\omega = 0$) is rather large
 328 ($u_s^* = 0.3 \text{ m/s}$) in comparison with the values of the literature ($u_s^* \approx 0.21 \text{ m/s}$ (Ho et al.,
 329 2011)). This discrepancy is so important that it can not be ascribed to the uncertainty of the
 330 measurements. We strongly believe that this is due to the finite size of the sand bed. Indeed,
 331 the length of the sand bed is expected to play a significant role in the initiation of the transport
 332 since the latter is triggered by events of low probability. A long bed will thus make the
 333 occurrence of such events more likely than for a short bed. It is hard to tell what would be
 334 the relevant bed length to get size-independent results. This issue is of significant importance
 335 and would deserve a specific study which is out of the scope of this article. Besides this, our
 336 results are in line with those from Hotta et al. (1984) concerning the linear increase with ω .
 337 However, the coefficient a_ω is about 10 times greater than that found by Hotta et al. (1984)
 338 for a sand bed with similar grain size (i.e., $D = 0.2 \text{ mm}$) but mixed with water and subsequent
 339 potential evaporation phenomena. These results thus suggest that the oil modifies quantitatively
 340 the cohesion strength but not qualitatively.

341 Interestingly, we can take advantage of the relationship from McKenna-Neuman and Nickling
 342 (1989) (cf Eq. 4) to get an estimation of the strength of the cohesion force in terms of
 343 the cohesion number. Plugging Eq. 10 in Eq. 4 yields:

$$Co \approx \frac{a_\omega \omega}{3} (2 + a_\omega \omega) \quad (11)$$

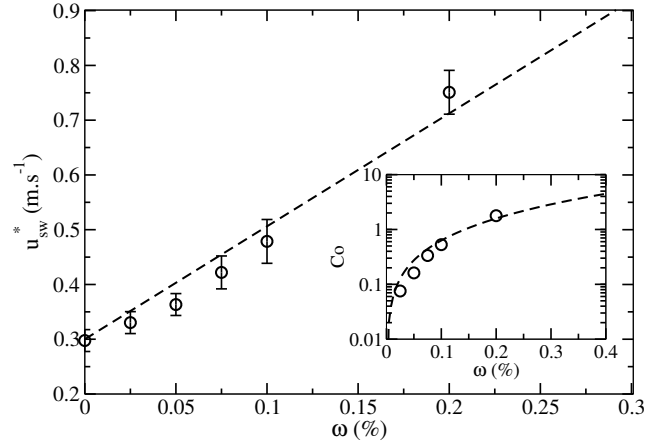


Figure 3. Static threshold u_{sw}^* as a function of the liquid content ω . The dash line corresponds to a linear fit to the data (see Eq. 10). Inset: The cohesion number Co as a function of the liquid content. The cohesion number Co is obtained from Eq. 4. The dash line corresponds to the predicted cohesion strength computed from the linear relationship between the threshold friction velocity and the liquid content:

$$Co = (a_\omega \omega / 3)(2 + a_\omega \omega).$$

344 The cohesion number varies between 0.01 to 2 (see the inset of Fig. 3). The magnitude of the
 345 cohesive strength can be compared with that produced by the capillary force: $Co_{cap} = \pi D \Gamma / mgD \approx$
 346 120 (with $D = 0.2 \text{ mm}$, $\rho_p = 2650 \text{ kg/m}^3$ and $\Gamma = 20.610^{-3} \text{ N/m}$). The estimated cohesion
 347 strength of the investigated sand beds is thus two order of magnitude less than the capillary
 348 force, which indicates that cohesion is probably driven by very thin films adsorbed on the grains
 349 rather than liquid capillary bridges.

350 4 Impact erosion

351 4.1 Upstream mass flux

352 To investigate the erosion by impact, we modified the upstream condition by prescribing
 353 a small but finite incoming mass flow rate $Q_{in} = 0.48 \text{ g/s}$ at the entrance of the wind-
 354 tunnel. With this prescribed incoming flux, experiments should be operated at a friction ve-
 355 locity equal or greater than 0.15 m/s . Below this value, the air flow is not able to transport
 356 the prescribed mass flux and deposition occurs, resulting in a decreasing mass flow rate with
 357 downstream distance.

358 The grains released at the entrance of the wind tunnel experience a saltation motion over
 359 a rigid and rough bed and are expected to be quickly in equilibrium with the flow. Their equi-
 360 librium downstream velocity, as well as their mean saltation height and length, are governed
 361 by the strength of the flow. It is necessary to characterize the properties of the saltating grains
 362 when they impact the sand. Two important properties should be determined: the vertical flux
 363 Φ (i.e., the number of particles impacting per unit area) and the mean velocity u_p of the im-
 364 pacting particles. The impact erosion rate E depends on both quantities and can be expressed
 365 as

$$E = \Phi \times N_E(u_p, Co \dots), \quad (12)$$

366 where N_E is the average number of ejected grains per impact produced by impacting particles
 367 having a mean velocity u_p . N_E is expected to depend as well on the cohesion number Co . We
 368 should emphasize here that N_E is of course closely related to the number of ejected grains per
 369 impact determined in splash experiments (Beladjine et al., 2007) but it is different. Indeed, in
 370 splash experiments, the number of ejected grains per impact, $N_{ej}(\xi)$, is assessed for a well-

371 controlled impact velocity ξ . This is not the case in the present experiment where the impact-
 372 ing particles can exhibit a quite significant dispersion around the mean value u_p . We can infer
 373 $N_E(u_p)$ from $N_{ej}(\xi)$ if the distribution of the particle velocity is known. The calculation is
 374 done in Appendix A where a Gaussian velocity distribution is assumed.

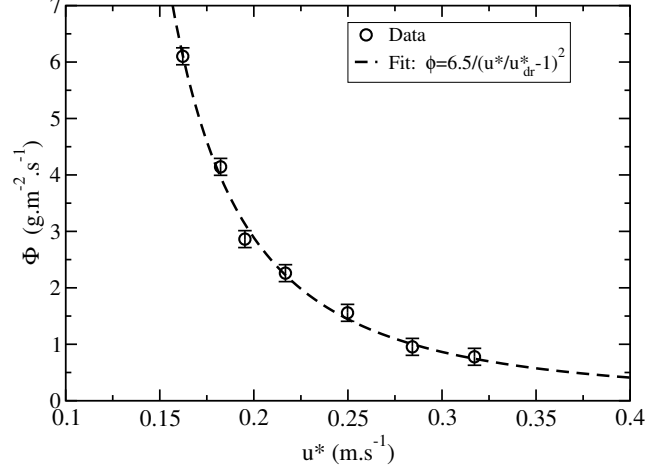


Figure 4. Impact flux Φ as a function of the shear velocity u^* for a given incoming flux $Q_{in} = 0.48$ g/s.

375 The mean velocity of the impacting particles can be estimated from the measurements
 376 made by Ho (2012). He reported that the equilibrium velocity of saltating particles over a rigid
 377 bed is completely determined by the flow strength and proposed the following empirical rela-
 378 tionship for 0.2 mm sand grains,

$$\frac{u_p}{\sqrt{gd}} \approx 80 (u^*/u_{reb}^* - 1), \quad (13)$$

379 where u_{reb}^* is the critical shear velocity to sustain a steady saltation motion of a single grain
 380 on a rigid and rough bed with $u_{reb}^* \approx 0.128$ m/s. This critical friction velocity can be inter-
 381 preted as the rebound threshold on a rigid bed (Pächt et al., 2020, 2021). The relation holds
 382 as long as the flow is far from being saturated, that is, when the saltation layer is so dilute that
 383 the sand grains do not have any feed-back effect on the flow.

384 The impact flux Φ was directly measured by trapping the impacting grains at the loca-
 385 tion of the sand bed. To do so, we replaced the sand bed by an equivalent surface acting as
 386 a sand trap. The container used for the sand bed was filled instead with a viscous liquid (sun-
 387 flower oil). Doing so, we avoid both evaporation of the liquid and ensure an efficient trapping.
 388 The flux is assessed by the same system of weighing used to determine the erosion rate. Fig. 4
 389 presents the variation of the vertical flux Φ as a function of the shear velocity u^* for a pre-
 390 scribed incoming mass flux $Q_{in} = 0.48$ g/s. As expected, the latter decreases with increas-
 391 ing shear velocity and the decreasing trend is well captured by

$$\Phi \propto \frac{Q_{in}}{(u^*/u_{reb}^* - 1)^2}. \quad (14)$$

392 This is in agreement with the findings from Ho et al. (2011). In a steady and fully developed
 393 state of transport, the impact flux is given by $\Phi = Q/l_{salt}$ where l_{salt} is the mean saltation length
 394 and Q the mass flow rate. Ho et al. (2011) showed that over a rigid and rough bed, the mean
 395 saltation length scales as $(u^*/u_{reb}^* - 1)^2$, which is fully compatible with our results on Φ .

396

4.2 Experimental results

397

398

399

400

401

402

As the impacting flux is varying in our experiments, the impact erosion rate E is rescaled by the impacting flux Φ and can be interpreted as the mean number of particles ejected by a single impact. The experimental data are reported in Fig. 5 where we display the rescaled erosion rate E/Φ as a function of the friction velocity for 4 different cohesion strengths. We can clearly identify a critical friction velocity u_d^* for impact erosion. We interpret this critical velocity as the dynamic transport threshold.

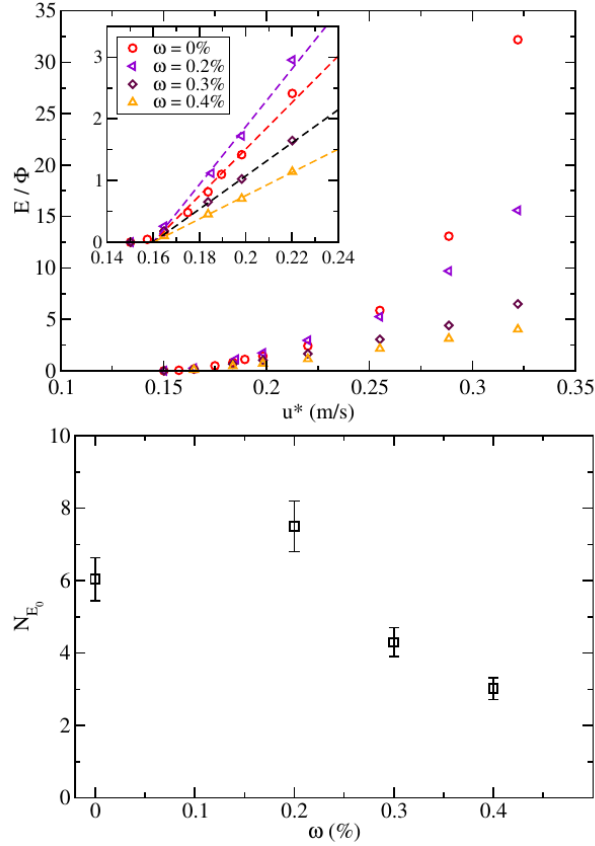


Figure 5. (a) Rescaled impact erosion rate E/Φ as a function of the friction velocity for different cohesion strengths. Inset: Magnification of the region close to the threshold, underlining the linear trends of the impact erosion rate. (b) N_{E_0} as a function of the liquid content ω (see Eq. 15).

403

404

405

406

407

408

409

410

411

412

413

The first salient result is that the dynamic transport threshold is insensitive to the level of cohesion of the bed: $u_d^* \approx 0.16$ m/s. This threshold value is consistent with those found in the literature in the context of cohesionless sand beds. For example, Ho et al. (2011) reported a dynamic threshold $u_d^* \approx 0.17$ m/s for 0.2 mm cohesionless sand, consistent with our value. In contrast to what found for the aerodynamic threshold, this agreement suggests that the outcomes concerning impact erosion are not much sensitive to the size of the sand bed sample. Interestingly, the value of the dynamic threshold corresponds to a critical mean particle velocity $u_{p,0} \approx 20\sqrt{gd}$. According to Creyssels et al. (2009) and as shown in appendix A, we can infer from $u_{p,0}$ the critical impact velocity ξ_0 to trigger the erosion process: $\xi_0 \approx 2u_{p,0} \approx 40\sqrt{gd}$. The obtained value for ξ_0 is in agreement with that found from model collision experiments with 6 mm plastic beads (Beladjine et al., 2007).

The second salient result is that close to the threshold, the rescaled impact erosion rate E/Φ obeys an linear law

$$\frac{E}{\Phi} \approx N_{E_0}(\omega) \left(\frac{u^*}{u_d^*} - 1 \right), \quad (15)$$

where N_{E_0} is a fitting parameter (see Fig. 5.b). Two important comments follow. Using the relationship between the mean particle velocity and the air friction velocity (cf Eq. 13), the rescaled impact erosion rate E/Φ can be expressed in terms of the mean particle velocity of the impacting grains:

$$\frac{E}{\Phi} \approx \frac{N_{E_0}(\omega)}{5} \left(\frac{u_p}{u_{p,0}} - 1 \right). \quad (16)$$

To derive this relationship, we used that $u_d^*/u_{reb}^* \approx 5/4$. The critical velocity $u_{p,0}$ can be interpreted as the mean particle velocity at which the replacement capacity is equal to 1. We found that the critical mean particle velocity $u_{p,0}$ is not modified by the cohesion strength of the packing. Only, the efficiency of the impact erosion rate encoded through the quantity N_{E_0} is altered by the cohesion. N_{E_0} decreases significantly for liquid contents ω equal or greater than 0.3% (i.e., $Co \geq 3$). We can note that for $\omega = 0.2$, the coefficient N_{E_0} is a bit greater than for cohesionless beds (see Table 1). This may be probably explained by the fact that the packing fraction of the cohesive packing is slightly smaller than the cohesionless one. The bed is therefore looser and may enhance the erosion by impact.

The second important point to mention is that the linear behavior of the impact erosion rate E with the air friction velocity or mean particle velocity is observed only close to the dynamic threshold (i.e., $0.16 \text{ m/s} < u^* < 0.22 \text{ m/s}$). Far above the threshold, the increase becomes non-linear with a power-law greater than 1. Several plausible additional physical mechanisms may act in concert to increase the efficiency of the measured erosion rate at high friction velocity. An additional contribution may result from the direct aerodynamic erosion but also from a chain reaction process. Indeed, as the bed has a finite size, the ejected grains may rebound several times before leaving the bed. If the latter are sufficiently accelerated by the wind, they can trigger other ejection events as they hit the bed as in a chain reaction process. We believe that this process is responsible for the non-linear behavior of the erosion rate at high friction velocity.

5 Discussion and conclusion

With our original experimental set-up, we were able to assess the aerodynamic and impact thresholds in the context of the cohesive sand beds. Importantly, we used oil silicone instead of water to make the sand bed cohesive. This allows to get rid of the issue of water evaporation which makes difficult to control the cohesion properties of the bed in the course of time.

The first major experiment outcome is that the aerodynamic threshold friction velocity increases linearly with the liquid content, while the dynamic threshold remains unchanged with increasing cohesion strength, in the range of cohesion investigated so far (i.e., up to cohesion number $Co \approx 4.5$). We ascribe the invariance of the dynamic transport threshold with cohesion to the splash process and in particular to the fact that the critical impact velocity ξ_0 to trigger the ejection process is unaffected by cohesion in this range. A similar result was reported in numerical simulations of the impact process on cohesive granular packings by V. Ralarisoa et al. (2022). The numerical outcomes indicate that the critical impact velocity is unchanged as long as the cohesion number is less than 5. According to that prediction, an effect is expected to appear for liquid content ω equal or greater than 0.45%, which was not reached in our experiments. There are alternative explanations for the invariance of the dynamical threshold as proposed by Pahitz et al. (2021). They relate the dynamic threshold to the rebound threshold, which is indeed weakly dependent on the level of cohesion as reported in the numerical simulations by Comola, Gaume, et al. (2019).

The second feature is that the erosion by impact becomes less efficient for cohesion number equal or larger than 3 (N_{E_0} decreases when $Co \geq 3$) although the dynamic threshold re-

461 mains unchanged. According to the numerical outcomes by V. Ralaiarisoa et al. (2022), the
 462 splash process and its efficiency are not affected for cohesion number $Co \leq 5$, indicating a
 463 possible discrepancy between the experimental and numerical outcomes. However, as shown
 464 in Appendix A, the impact erosion rate E depends of course on the efficiency of the splash
 465 process but also on the nature of the velocity distribution of the impact particles. Increasing
 466 the air flow velocity may affect the velocity distribution. As an example, an increase of the
 467 vertical impact velocity fluctuation (i.e., T_y) results in the reduction of the erosion rate (see
 468 Eq.A10). We can not therefore conclude definitively about the cause of the decrease of N_{E_0}
 469 for cohesion number between 0.3 and 0.5. A decreasing efficiency of impact erosion rate should
 470 have important consequences on the equilibrium length to reach the equilibrium mass flux. In
 471 particular, this would lead to an augmentation of the equilibrium length.

472 The third important result is that aerodynamic erosion rate shows an exponential increase
 473 with the friction velocity both for cohesionless and cohesive beds. This raises the question of
 474 setting an appropriate criterion to define a meaningful aerodynamic threshold. To circumvent
 475 this difficulty, we used a criterion based on a critical value of the erosion rate in compliance
 476 with the weigh scale accuracy. In contrast, the impact erosion rate obeys a linear law with the
 477 friction velocity.

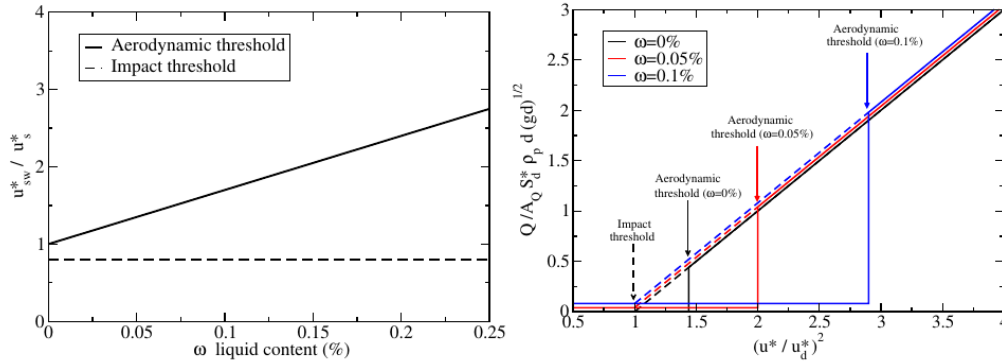


Figure 6. (a) Aerodynamic and Impact thresholds as a function of the liquid content. (b) Conjectured mass transport rate at equilibrium and bi-stable domain for various liquid content: This graph illustrates the increase of the range of the bi-stable domain (i.e., $u_d^* < u^* < u_{su}^*$) with increasing cohesion. Here we conjectured that the mass transport law at equilibrium is unchanged for cohesive granular beds (see Eq. 5).

478 The most impressive effect of the cohesion is to increase the difference between the static
 479 and dynamic threshold (see Fig. 6.a). A practical consequence of this outcome is the develop-
 480 ment of strong hysteretic behaviors due to bi-stability if the wind friction velocity lies be-
 481 tween the static and dynamic threshold. Indeed, for increasing cohesion strength, the range
 482 of the bi-stable domain strongly increases (see Fig. 6b). As a consequence, the experimen-
 483 tal assessment of the mass flow rate in this bi-stable regime could lead to a large bias because
 484 the measurements may aggregate transport states of different nature according to the upstream
 485 boundary conditions.

486 An important issue to be addressed in the future is the determination of the maximum
 487 transport capacity of the wind in the context of cohesive sand beds (McKenna-Neuman & Mal-
 488 jaars, 1998; Davidson-Arnott et al., 2005). For cohesionless sand bed, the intensity of the sat-
 489 urated mass flux depends on the distance of the Shields number S^* from the dynamic thresh-
 490 old Shields number S_d^* multiplied by the dynamic threshold friction velocity u_d^* (see Eq. 5).
 491 As the dynamic threshold is insensitive to cohesion at least in a definite range of cohesion strength
 492 (i.e., $Co < 2$), our expectation is that the saturated flux should remain independent of the bed

493 cohesion as illustrated in Fig. 6.b and suggested by the numerical simulations from Comola,
 494 Gaume, et al. (2019). Experimental verifications of this conjecture are currently under inves-
 495 tigation.

496 **Data Availability Statement**

497 The data set corresponding to Figures 2, 3, 4 and 5 are available as Supporting Information
 498 at "https://doi.org/10.5281/zenodo.7100605" (Besnard et al., 2022). The file ReadMe indicates
 499 how the data are displayed.

500 **Acknowledgments**

501 We acknowledge the support of the French Research National Agency through the project ANR-
 502 17-CE01-0014.

503 **Appendix A Calculation of the impact erosion rate**

504 We derive here the expression of the impact erosion rate assuming that the velocity dis-
 505 tribution of the impact particles as well as the features of the ejection process are prescribed.

506 Based on the numerical simulations and experiments (Oger et al., 2005; Beladjine et al.,
 507 2007), we assume that the number of particles, including the rebound, resulting from a im-
 508 pact at velocity ξ is given by:

$$N(\xi) = \begin{cases} 1 + N_{ej} & \text{if } \xi > \xi_0 \\ 1 & \text{if } \xi_c \leq \xi \leq \xi_0 \\ 0 & \text{if } \xi \leq \xi_c, \end{cases} \quad (A1)$$

509 with

$$N_{ej}(\xi) = N_0(1 - (A - B \sin^2 \theta)^2)(\xi/\xi_0 - 1) \quad (A2)$$

510 ξ_0 is the critical velocity below which there is no ejection and N_{ej} is the number of ejected
 511 grains per impact when $\xi \leq \xi_0$. θ is the impact angle measured from the horizontal and The
 512 measurements for a cohesionless granular packing give $N_0 = 13$, $A = 0.86$, $B = 0.72$, and
 513 $\xi_0 = 40 \sqrt{gd}$ (Beladjine et al., 2007). This relation indicates that the number of ejected par-
 514 ticles is the product of a function that depends only on the impact angle and a linear function
 515 of the impact velocity above a threshold value ξ_0 . If the velocity of the impacting particle is
 516 less than ξ_c , the impacting particle is captured by the bed ($\xi_c \approx \sqrt{gd}$),

517 As done in Creyssels et al. (2009), it is reasonable to assume that the velocity of the im-
 518 pacting grains obeys a half-Gaussian distribution (i.e., $\xi_y < 0$):

$$f = \frac{c_0}{\pi \sqrt{T_x} \sqrt{T_y}} e^{-(\xi_x - u_p)^2 / 2T_x} e^{-\xi_y^2 / 2T_y}, \quad (A3)$$

519 where ξ_x and ξ_y are the horizontal and vertical components of the impact velocity $\vec{\xi}$ (ξ_y is neg-
 520 ative for impacting particle), c_0 is the concentration of the impacting particle at the bed, u_p
 521 is the mean horizontal velocity of the impacting particles, $T_x = \langle \xi_x^2 \rangle$ and $T_y = \langle \xi_y^2 \rangle$.

522 With these assumptions, the impact erosion rate reads:

$$E = m \int_{\xi_y < 0} (N - 1) \xi_y f(\xi) d\xi_x d\xi_y \quad (A4)$$

523 Following Creyssels et al. (2009), the erosion rate can be split into two contributions: the rate
 524 of ejected grains, E_{ej} , and the rate of grains trapped by the bed, E_{loss} , which are given respec-
 525 tively by

$$E_{ej} = m \int_{\xi_y < 0, \xi > \xi_0} f(\vec{\xi}) N_{ej}(\vec{\xi}) |\xi_y| d\vec{\xi}, \quad (A5)$$

$$E_{loss} = m \int_{\xi_y < 0, \xi < \xi_c} f(\vec{\xi}) |\xi_y| d\vec{\xi}. \quad (A6)$$

526 The result of the integration yields (Creyssels et al., 2009):

$$E_{ej} \approx \frac{mc_0 N_0}{\pi \sqrt{T_x T_y}} \frac{T_x^3}{u_p (\xi_0 - u_p)^2} e^{-(\xi_0 - u_p)^2 / 2T_x} \times \left(1 - A^2 + AB \sqrt{\frac{2\pi T_x}{\xi_0 u_p}} \right), \quad (A7)$$

$$E_{loss} \approx 74 \frac{mc_0}{\pi \sqrt{T_x T_y}} \xi_c^3 e^{-u_p^2 / (2T_x)}. \quad (A8)$$

527 The impact erosion rate vanishes when E_{ej} balances exactly E_{loss} . Assuming that $u_p \gg$
528 $\sqrt{T_x}$, the balance reduces to (Creyssels et al., 2009):

$$u_p \approx \frac{\xi_0}{2} \quad (A9)$$

529 This means that the erosion rate vanishes when the mean particle velocity of the impacting
530 particle equals the critical velocity $u_{p,0} \approx \xi_0/2$. The critical mean particle velocity is thus com-
531 pletely linked to the critical impact velocity ξ_0 to trigger the ejection process. A linear expan-
532 sion around $u_{p,0}$ provides an approximate for the erosion rate which yields to first order:

$$E \approx \phi N_0 \left(1 - A^2 + AB \sqrt{\frac{4\pi T_x}{\xi_0^2}} \right) \frac{2T_x^{3/2} e^{-\xi_0^2 / 8T_x}}{\pi \xi_0 T_y} \left(\frac{u_p}{u_{p,0}} - 1 \right) \quad (A10)$$

533 where $\phi = mc_0 \sqrt{T_y}$ is the vertical impacting mass flux. If we take a typical value of T for
534 saltation transport on a rigid and rough bed (Ho, 2012) ($T_x \approx T_y \approx 200 \text{ gd}$), we get: $E \approx$
535 $0.5 \phi (u_p/u_{p,0} - 1)$ which is of the same order of magnitude as what found in the experiments
536 for cohesionless sand bed ($E(\omega = 0) \approx \phi (u_p/u_{p,0} - 1)$; see Eq. 16).

537 References

- 538 Andreotti, B., Claudin, P., Iversen, J. J., Merrison, J. P., & Rasmussen, K. R. (2021).
539 A lower-than-expected saltation threshold at martian pressure and below. *Pro-*
540 *ceedings of the National Academy of Sciences*, 118(5), e2012386118. doi:
541 10.1073/pnas.2012386118
- 542 Andreotti, B., Claudin, P., & Pouliquen, O. (2010). Measurements of the aeolian sand trans-
543 port saturation length. *Geomorphology*, 123, 343-348.
- 544 Bagnold, R. A. (1941). The physics of blown sand and desert dunes. *Methuen, New York*.
- 545 Beladjine, D., Ammi, M., Valance, A., & Oger, L. (2007). Collision process between an inci-
546 dent bead and a three-dimensional granular packing. *Physical Review E*, 75, 061305.
- 547 Belly, P. (1962). Sand movement by wind, united states army corps of engineers. *Coastal*
548 *Engineering Research Center, Technical Memorandum, Washington, Vol I*.
- 549 Besnard, J., Dupont, P., Ould El Moctar, A., & Valance, A. (2022). Aeolian erosion thresh-
550 olds for cohesive sand [data set]. *Zenodo*. doi: 10.5281/zenodo.7100605
- 551 Bisal, F., & Hsieh, J. (1966). Influence of moisture on erodibility of soil by wind. *Soil sci-*
552 *ence*, 102, 103-146.
- 553 Chepil, W. (1956). Influence of moisture on erodibility of soil by wind. *Soil science Society*
554 *Proceedings*, 20, 288-292.
- 555 Claudin, P., & Andreotti, B. (2006). A scaling law for aeolian dunes on mars, venus, earth,
556 and for subaqueous ripples. *Earth and Planetary Science Letters*, 252(1), 30-44.
- 557 Comola, F., Gaume, J., Kok, J. F., & Lehning, M. (2019). Cohesion-induced enhancement of
558 aeolian saltation. *Geophysical Research Letters*, 46(10), 5566-5574.
- 559 Comola, F., Kok, J. F., Chamecki, M., & Martin, R. L. (2019). The intermittency of wind-
560 driven sand transport. *Geophysical Research Letters*, 46(22), 13430-13440.
- 561 Cornelis, W. M., Gabriels, D., & Hartmann, R. (2004a). A conceptual model to predict the
562 deflation threshold shear velocity as affected by near-surface soil water. *Soil Science*
563 *Society of America Journal*, 68(4), 1154-1161.
- 564 Cornelis, W. M., Gabriels, D., & Hartmann, R. (2004b). A conceptual model to predict the
565 deflation threshold shear velocity as affected by near-surface soil water. *Soil Science*
566 *Society of America Journal*, 68(4), 1162-1168.

- 567 Creyssels, M., Dupont, P., Ould El Moctar, A., Valance, A., Cantat, I., Jenkins, J. T., . . . Ras-
568 mussen, K. R. (2009). Saltating particles in a turbulent boundary layer : experiment
569 and theory. *Journal of Fluid Mechanics*, *625*, 47-74.
- 570 Davidson-Arnott, R. G. D., MacQuarrie, K., & Aagaard, T. (2005). The effect of wind gusts,
571 moisture content and fetch length on sand transport on a beach. *Geomorphology*, *68*,
572 115-129.
- 573 Davidson-Arnott, R. G. D., Yang, Y., Ollerhead, J., Hesp, P. A., & Walker, I. J. (2008). The
574 effects of surface moisture on aeolian sediment transport threshold and mass flux on a
575 beach. *Earth Surface Processes and Landforms*, *33*(1), 55-74.
- 576 Duran, O., Claudin, P., & Andreotti, A. (2011). On aeolian transport: Grain-scale interac-
577 tions, dynamical mechanism and scaling laws. *Aeolian Research*, *3*, 243-270.
- 578 Han, Q., Qu, J., Zhang, K., Zu, R., Niu, Q., & Liao, K. (2009). Wind tunnel investigation of
579 the influence of surface moisture content on the entrainment and erosion of beach sand
580 by wind using sands from tropical humid coastal southern china. *Geomorphology*,
581 *104*(3), 230-237.
- 582 Ho, T. D. (2012). *Experimental study of saltating particles in a turbulent boundary layer*
583 (Unpublished doctoral dissertation). University of Rennes 1.
- 584 Ho, T. D., Valance, A., Dupont, P., & Ould El Moctar, A. (2011). Scaling laws in aeolian
585 sand transport. *Physical Review Letters*, *106*, 094501.
- 586 Hotta, S., Kubota, S., Katori, S., & Horikawa, K. (1984). Sand transport by wind on a wet
587 sand surface. In *Coastal engineering 1984* (p. 1265-1281).
- 588 Jenkins, J., & Valance, A. (2014). Periodic trajectories in aeolian sand transport. *Physics of*
589 *Fluid*, *26*, 073301.
- 590 Kok, J., & Rennó, N. (2009). A comprehensive numerical model of steady state saltation.
591 *Journal of Geophysical Research. Atmospheres*, *114*, D17204.
- 592 Louge, M. Y., Valance, A., elMoctar, A. O., Xu, J., Hay, A. G., & Richer, R. (2013). Tem-
593 perature and humidity within a mobile barchan sand dune, implications for microbial
594 survival. *Journal of Geophysical Research: Earth Surface*, *118*(4), 2392-2405. doi:
595 <https://doi.org/10.1002/2013JF002839>
- 596 Louge, M. Y., Valance, A., Mint Babah, H., Moreau-Trouv, J.-C., Ould el Moctar, A.,
597 Dupont, P., & Ould Ahmedou, D. (2010). Seepage-induced penetration of water
598 vapor and dust beneath ripples and dunes. *Journal of Geophysical Research: Earth*
599 *Surface*, *115*(F2). doi: <https://doi.org/10.1029/2009JF001385>
- 600 Louge, M. Y., Valance, A., Xu, J., Ould el Moctar, A., & Chasle, P. (2022). Water vapor
601 transport across an arid sand surfacenon-linear thermal coupling, wind-driven pore
602 advection, subsurface waves, and exchange with the atmospheric boundary layer.
603 *Journal of Geophysical Research: Earth Surface*, *127*(4), e2021JF006490.
- 604 Martin, R. L., & Kok, J. F. (2018). Distinct thresholds for the initiation and cessation of ae-
605olian saltation from field measurements. *Journal of Geophysical Research: Earth Sur-*
606 *face*, *123*(7), 1546-1565.
- 607 McKenna-Neuman, C., & Maljaars, M. S. (1998). A wind tunnel study of the influence of
608 pore water on aeolian sediment transport. *Journal of Arid Environments*, *39*, 403-419.
- 609 McKenna-Neuman, C., & Nickling, W. G. (1989). A theoretical and wind tunnel investiga-
610 tion of the effect of capillary water on the entrainment of sediment by wind. *Canadian*
611 *Journal of Soil Science*, *69*(1), 79-96.
- 612 Namikas, S. L., & Sherman, D. J. (1995). A review of the effects of surface moisture con-
613 tent on aeolian sand transport. In V. P. Tchakerian (Ed.), *Desert aeolian processes* (pp.
614 269–293). Dordrecht: Springer Netherlands.
- 615 Oger, L., Ammi, M., Valance, A., & Beladjine, D. (2005). Discrete element method to study
616 the collision of one rapid sphere on 2d and 3d packings. *The European Physical Jour-*
617 *nal E*, *17*, 467-476.
- 618 Pähtz, T., Clark, A. H., Valyrakis, M., & Durn, O. (2020). The physics of sediment transport
619 initiation, cessation, and entrainment across aeolian and fluvial environments. *Reviews*
620 *of Geophysics*, *58*(1), e2019RG000679.
- 621 Pähtz, T., Liu, Y., Xia, Y., Hu, P., He, Z., & Tholen, K. (2021). Unified model of sediment

- 622 transport threshold and rate across weak and intense subaqueous bedload, windblown
 623 sand, and windblown snow. *Journal of Geophysical Research: Earth Surface*, 126(4),
 624 e2020JF005859.
- 625 Pähtz, T., Valyrakis, M., Zhao, X.-H., & Li, Z.-S. (2018). The critical role of the boundary
 626 layer thickness for the initiation of aeolian sediment transport. *Geosciences*, 8(9).
- 627 Ralaiarisoa, J.-L., Besnard, J.-B., Furieri, B., Dupont, P., Ould El Moctar, A., Naaim-Bouvet,
 628 F., & Valance, A. (2020, May). Transition from saltation to collisional regime in
 629 windblown sand. *Phys. Rev. Lett.*, 124, 198501.
- 630 Ralaiarisoa, V., Dupont, P., Moctar, A. O. E., Naaim-Bouvet, F., Oger, L., & Valance, A.
 631 (2022, May). Particle impact on a cohesive granular media. *Phys. Rev. E*, 105, 054902.
 632 doi: 10.1103/PhysRevE.105.054902
- 633 Ralaiarisoa, V. J.-L. (2020). *Influence de la cohésion sur le transport éolien de particules :
 634 application au sable humide et à la neige* (Unpublished doctoral dissertation). Univer-
 635 sité Rennes 1.
- 636 Selmani, H., Valance, A., Ould El Moctar, A., Dupont, P., & Zegadi, R. (2018). Aeolian sand
 637 transport in out-of-equilibrium regimes. *Geophysical Research Letters*, 45(4), 1838-
 638 1844.
- 639 Shao, Y., & Lu, H. (2000). A simple expression for wind erosion threshold friction velocity.
 640 *Journal of Geophysical Research: Atmospheres*, 105(D17), 22437-22443. doi: [https://
 641 doi.org/10.1029/2000JD900304](https://doi.org/10.1029/2000JD900304)
- 642 Stout, J. E., & Zobeck, T. M. (1996). The wolfforth field experiment: A wind erosion study.
 643 *Soil Science*, 161 (9), 616-632.
- 644 Valance, A., Rasmussen, K. R., Ould El Moctar, A., & Dupont, P. (2015). The physics of ae-
 645olian sand transport. *Comptes Rendus Physique*, 16(1), 105-117.